the solar spectrum, S. Johansson for computations of the neutral iron spectrum in the region, R. C. M. Learner for researching his laboratory spectra of iron, B. Farmer for providing the ATMOS spectra, and J. Sauval for calculating a synthetic spectrum of CN solar absorption. We also acknowledge B. Bezard for carrying out detailed computations of the effect of the thermal radiation on the spectral lines of HDO and helpful discussions with J. Fox and J. Kasting on the problem of H escape. This research was supported in part by NASA grants NSG-7499 and NGR33015141.

17 December 1987; accepted 6 May 1988

Anomalous Upstream Retroflection in the Agulhas Current

J. R. E. LUTJEHARMS AND R. C. VAN BALLEGOOYEN

The Agulhas current, the major western boundary current of the Southern Hemisphere, plays a crucial role in the water mass balance of the world oceans by controlling the transfer of thermocline water from the Indian to the Atlantic ocean systems. The main mechanism for such transfer is through the shedding of large rings of warm water at the Agulhas retroflection south of Africa. On the basis of satellite imagery and drifter tracks, anomalous reversals of the current are observed to occur far upstream of its characteristic retroflection location. The observations agree with results of an inertial jet model of the current. These anomalous reversals probably cause abrupt and major changes in the fluxes south of Africa and thus in the rate of ring shedding. This unusual flow bimodality in a major component of the global ocean heat transport system could have important climatic implications.

THE AGULHAS CURRENT DOMINATES the circulation pattern of the southwest Indian Ocean. It derives most of its water from the Mozambique channel (*1*), from east of Madagascar (*2, 3*) and from recirculation in a southwest Indian Ocean subgyre (*1, 2*). It reaches its full stature at about the latitude of Durban (Fig. 1) and closely follows the shelf edge of the southern African continent for most of its subsequent downstream path (*4*). On overshooting the southern tip of the continent, it retroflects in a reversal (*5*) that carries most of its warm, saline water back to the south Indian Ocean. The retroflection loop is an unstable configuration (*6*) that causes a large Agulhas ring to occasionally pinch off (*7*). These rings, described as the most intense observed anywhere (*8*), drift into the South Atlantic Ocean. Ring shedding occurs, on average, about nine times per year (*9*), which leads to a substantial transfer of energy and water from the Indian to the Atlantic ocean systems. This exchange of water has important climatic implications (*10, 11*).

The total flux of warm Indian Ocean water into the Atlantic by way of ring shedding is most likely a function of the volume flux of the Agulhas current (*12*). Various models of the current (*12*) suggest that perturbations in the flow may precipitate ring formation or influence the rate of ring shedding. The Agulhas current upstream of Port Elizabeth (Fig. 1), however, has a remarkably stable path configuration (*4*), flow rate (*13*), and mass transport (*14*) for a western boundary current.

We have scrutinized 11 years of thermal infrared satellite images of the southwest Indian Ocean to test the hypothesis (*15*) that the configuration of the southwest Indian Ocean subgyre might lead to an occasional eastward leakage of water from the Agulhas current location at a position far upstream of its usual retroflection location (*16*). This circulation system lends itself particularly well to investigations by thermal infrared remote sensing because sea-surface temperature contrasts are high in this area and the surface thermal expression of the Agulhas current is strongly coherent with its deeper flow (*7*).

This investigation revealed that significant leakage or virtually total retroflection of Agulhas current water occurred at about the longitude of Port Elizabeth (25°E) two to three times per year, on average (Fig. 1). These events had a typical duration of 3 to 6 weeks. The event that is partly shown in Fig. 2 lasted for more than 2 months. These periods are long enough for a significant part of the total flow to be diverted. The occurrence of persistent cloudiness over the area for long periods during which the sea surface was either partially or totally obscured implies that this assessment of the incidence of upstream reversals on the basis of satellite images is probably an underestimate.

A few drift tracks of free-drifting buoys describe such instances of upstream reversal (Fig. 2). The track of buoy 74625 south of Port Elizabeth simulates the disposition of the eastward warm water outflow from the Agulhas current which commenced a few days before the buoy reached the area. Sea-surface temperatures measured by the buoy were consistently higher than 20°C, which indicates that the buoy was continuously in surface water of the Agulhas current. The drift track for a buoy that was placed a number of years previously describes a similar current configuration (Fig. 2) somewhat farther to the west. These drift patterns present circumstantial evidence for the existence of upstream retroflections.

In two instances the area was sufficiently cloud-free over an extended period to ob-

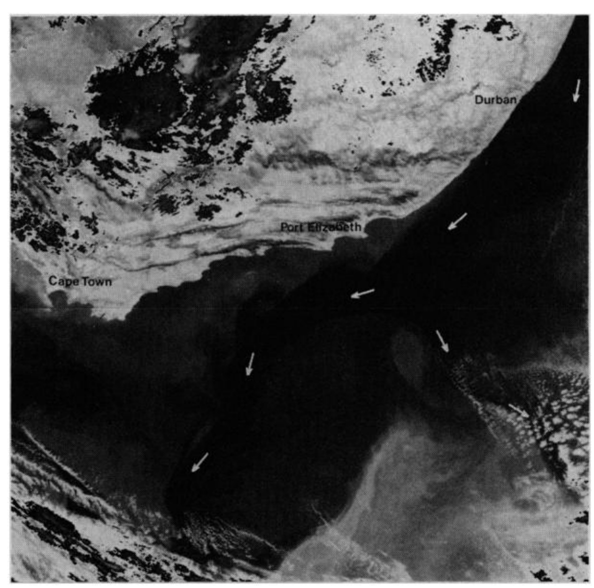

Fig. 1. Portrayal of an upstream retroflection of part of the Agulhas current in the vicinity of Port Elizabeth. This thermal infrared image is from the advanced very high resolution radiometer on board the NOAA (National Oceanic and Atmospheric Administration) satellite for 13 May 1983. Warm water is in darker hues. South of Port Elizabeth the Agulhas current is located seaward of its normal track and a clear bifurcation of warm water flow is apparent. The distance between Port Elizabeth and Cape Town is about 700 km.

National Research Institute for Oceanology, Council for Scientific and Industrial Research, P.O. Box 320, Stellenbosch 7600, South Africa.

serve a sequence of kinematic events which preceded and followed an upstream retroflection. In both cases, an extreme solitary meander in the Agulhas current (*17*) was observed to progress downstream while the Agulhas return current (*18*), forced by the Agulhas Plateau, was noted to lie landward of its mean position. When the meander in the Agulhas current approached the vicinity of the Agulhas Plateau, we infer that high horizontal shear between the meander and the Agulhas return current led to their amalgamation and a partial upstream retroflection in the current. This newly created loop then progressed downstream at a rate similar to that of the parent meander.

All observed leakage events started at about the same geographic location, 25°E, which suggests that a single mechanism may cause the upstream retroflection. In an attempt to identify this mechanism we modeled the Agulhas current by representing it as a free inertial jet. We have used the model of steady-state conservation of potential vorticity (*19*). We assume that the current can be regarded as a narrow filament of rapidly flowing water that moves steadily and without friction through a region of geostrophic flow (*19*).

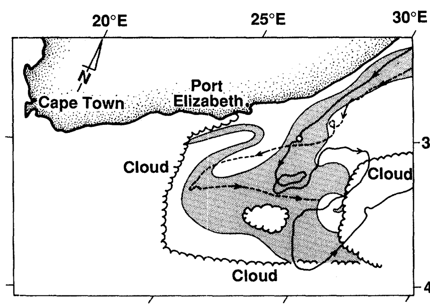

Fig. 2. Interpretive line drawing of a thermal infrared satellite portrayal of an upstream reversal of the Agulhas current. The image used was from METEOSAT II for 20 April 1981. Tracks of two free-drifting weather buoys have been superimposed (*21*). The solid line is for buoy 74625; its position on 30 April 1981 is indicated by an open circle on the track. The broken line represents the drift track of a buoy that was launched in 1973 (*22*). The Agulhas current usually retroflects about 500 km southwest of Cape Town.

Results of a number of parameter configurations are presented in Fig. 3. The parameter values that we used are realistic according to all measurements currently available. The parameter ranges exceed those measured so that modeling results should be representative of what occurs in the ocean and not be an artifact of a narrow range of values. All current trajectories were started off Durban at 30°S in a water depth of 1000 m (Fig. 3). This location corresponds closely to the mean path location for the current in this area (*4*). A vertical velocity profile was used that approximates the observed profile (*14*). Values of bottom velocity were chosen to lie between 5 and 10 cm/s; initial surface velocities were between 160 and 200 cm/s, which are comparable with published data of 160 cm/s (*13*). A width of 120 km was used for the current to match its established volume transports (*14*).

In all cases where lateral movement is such that the jet crosses over the northern extension of the Agulhas Plateau (Fig. 3) it retroflects. The shortest distances between the 1000-m isobath of the continental shelfbreak, where the Agulhas current is usually located, and the 4000-m and 3500-m isobaths of the plateau are 150 and 250 km, respectively (Fig. 3). Results of the application of the free inertial jet model therefore imply that shoaling of the offshore bottom topography of the Agulhas Plateau induces the Agulhas current to retroflect at 25°E when seaward meandering of the current exceeds 200 km. The geographic location of retroflection agrees with the position of all upstream reversals that were observed in satellite imagery and buoy drift tracks. Although the physics controlling the flow were simplified in the inertial jet model, the model's demonstrated ability to simulate bottom influences on the path of the Agulhas current (*12*) gives us confidence that the upstream reversal is indeed bathymetrically induced.

Extreme lateral meanders in the Agulhas current with amplitudes that exceed 200 km are rare (*17*). Most observed meanders of this size have been identified as "Natal pulses," which are large, solitary meanders caused by upstream vortex shedding (*17*). Eddies formed in the lee of the sharp coastal offset at about 29°S, the Natal bight, are shed intermittently and move downstream inshore of the Agulhas current. They force large but transient path divergences on its flow path. The amplitudes of these pulses range between 50 and 230 km; pulses are observed on some part of the current at least 17% of the time (*17*). An estimated 20% of these pulses would have sufficient amplitude at the longitude of Port Elizabeth to cause retroflections of the current here as implied by the free inertial jet model.

The satellite and drifter observations presented in this report are for the upper ocean layers only; even though these are usually representative of deep layers in this area (*5, 7, 11*), no deep measurements of an upstream retroflection are currently available that would allow the vertical extent to be determined. Results of the inertial jet model and of previous cruises in the area (*15*) strongly suggest, however, that upstream retroreflections are not a surface phenomenon only.

Every one of the world's western boundary currents exhibits certain singular kinematic characteristics because of their different geographical locations and in particular because of the distinct adjacent coastal and bathymetric morphologies that are associated with each current. The upstream retroflection of the Agulhas current, induced by the downstream advance of a Natal pulse combined with the presence of an atypical offshore shallow area, the Agulhas Plateau, may represent an intermittent, major interruption in the volume flux; such an interruption has not been observed in any other western boundary current (*20*).

The effect of full or partial retroflections cannot be quantified at present. The inherent instability in the dynamics of the normal downstream retroflection (*6, 12*) suggests that even small perturbations in the total volume flux of the current, caused by upstream diversions, may trigger or dampen ring shedding into the South Atlantic ocean. The effects of this mechanism on heat flow to the Atlantic ocean may have climatic implications on a large scale.

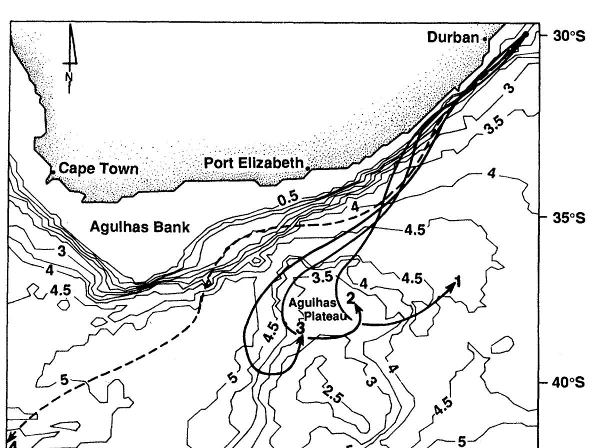

Fig. 3. A number of different current trajectories for the Agulhas current on the basis of a free inertial jet model. Parameter combinations for each flow path are for trajectory 1: $C = 1/2$, $V_T = 160$ cm/s, $V_B = 5$ cm/s; trajectory 2: $C = 1/2$, $V_T = 180$ cm/s, $V_B = 8$ cm/s; trajectory 3: $C = 1/2$, $V_T = 200$ cm/s, $V_B = 8$ cm/s; trajectory 4: $C = 1/2$, $V_T = 160$ cm/s, and $V_B = 7$ cm/s. V_T indicates current speed at the sea surface; V_B is the bottom current speed and C is the depth ratio between an upper, high-speed flow and a slower, bottom flow. The bathymetry is in steps of 500 m and is a digitized version of that by Simpson (*23*) at a 15-km grid spacing. The upstream retroflection that is forced by the Agulhas Plateau is evident.

REFERENCES AND NOTES

1. T. F. W. Harris, *Deep-Sea Res.* **19**, 633 (1972).
2. J. R. E. Lutjeharms, *J. Phys. Oceanogr.* **6**, 655 (1976).
3. ———, N. D. Bang, C. P. Duncan, *Deep-Sea Res.* **28**, 879 (1981).
4. M. L. Gründlingh, *S. Afr. Geogr. J.* **65**, 49 (1983).
5. N. D. Bang, *ibid.* **52**, 67 (1970); M. L. Gründlingh and J. R. E. Lutjeharms, *S. Afr. J. Sci.* **75**, 269 (1979); A. L. Gordon, J. R. E. Lutjeharms, M. L. Gründlingh, *Deep-Sea Res.* **34**, 565 (1987).
6. J. R. E. Lutjeharms, *S. Afr. J. Sci.* **77**, 231 (1981).
7. ——— and A. L. Gordon, *Nature* **325**, 138 (1987).
8. D. B. Olson and R. H. Evans, *Deep-Sea Res.* **33**, 27 (1986).
9. J. R. E. Lutjeharms and R. C. van Ballegooyen, *J. Phys. Oceanogr.*, in press.
10. A. L. Gordon, *J. Geophys. Res.* **91**, 5037 (1986).
11. ———, *Science* **227**, 1030 (1985).
12. J. R. E. Lutjeharms and R. C. van Ballegooyen, *Deep-Sea Res.* **31**, 1321 (1984); D. B. Boudra and W. P. M. de Ruijter, *ibid.* **33**, 447 (1986); H. W. Ou and W. P. M. de Ruijter, *J. Phys. Oceanogr.* **16**, 280 (1986); J. Darbyshire, *Rev. P. Appl. Geophys.* **101**, 208 (1972).
13. A. F. Pearce and M. L. Gründlingh, *J. Mar. Res.* **40**, 177 (1982).
14. M. L. Gründlingh, *Deep-Sea Res.* **27**, 557 (1980).
15. T. F. W. Harris and D. van Foreest, *ibid.* **25**, 549 (1978); C. P. Duncan, thesis, University of Hawaii (1970); J. Darbyshire, *Deep-Sea Res.* **11**, 781 (1964).
16. Satellite thermal infrared images collected since 1976 include products from METEOSAT I and II, TIROS N, NIMBUS 7, and NOAA 4 to NOAA 9. METEOSATs are geostationery with radiometer measurements between 10.5 and 12.5 μm and have a spatial resolution at nadir of 5 km. All others are polar orbiting with subsatellite track resolutions of about 1.5 km and measure in the range 10.5 to 11.5 μm. Daily images from the METEOSATs and about thrice-weekly images from the others were studied. In all cases, appropriate contrast enhancement had been carried out for the thermal range of the oceanic area under investigation.
17. M. L. Gründlingh, *J. Geophys. Res.* **84**, 3776 (1979); J. R. E. Lutjeharms and H. R. Roberts, *J. Geophys. Res.* **93**, 631 (1988).
18. T. F. W. Harris, *Nature* **227**, 1043 (1970).
19. B. A. Warren, *Tellus* **15**, 167 (1963); A. R. Robinson and P. P. Niiler, *ibid.* **19**, 269 (1967). The form of the equation used is

$$\frac{d^2y}{dx^2}\left[1+\left(\frac{dy}{dx}\right)^2\right]^{-3/2} - C_0 + C_2(y-y_0) - C_1(B-B_0) = 0$$

where x and y refer to the mean points in the stream, B_0 is the total ocean depth at the origin (x_0,y_0), C_0 is the curvature of the free inertial jet at the origin, C_1 is a constant that equals $10^{10}f_0T/M$ where f_0 is the inertial frequency, T is a bulk value for the integrated volume transport across unit depth of the stream near the bottom, and M is the integrated momentum transport across the section of the stream. C_2 is also a constant, $10^{12}\beta V/M$, where β equals df/dy at any particular latitude, f is the Coriolis parameter, and V is the integrated volume transport. The numerical method of calculation is in (*12*).
20. D. Halkin and T. Rosby, *J. Phys. Oceanogr.* **15**, 1439 (1985); F. Schott and R. Zantopp, *Science* **227**, 305 (1985).
21. These buoys were all spar-shaped and equipped with window-shade drogues. They measured air and sea temperature and reported via satellite. No confirmation is available that drogues were still attached during the movement that is depicted in Fig. 2, but experimental evidence has shown that drogues have little influence on drift behavior [A. D. Kirwan, G. McNally, M.-S. Chang, R. Molinary, *J. Phys. Oceanogr.* **5**, 361 (1978)].
22. C. C. Stavropoulos and C. P. Duncan, *J. Geophys. Res.* **79**, 2744 (1974).
23. E. S. W. Simpson, Chart 125A Bathymetry (National Research Institute for Oceanology, Stellenbosch, South Africa, 1974).

24 December 1987; accepted 5 April 1988

Regeneration of Sensory Hair Cells After Acoustic Trauma

Jeffrey T. Corwin and Douglas A. Cotanche

Any loss of cochlear hair cells has been presumed to result in a permanent hearing deficit because the production of these cells normally ceases before birth. However, after acoustic trauma, injured sensory cells in the mature cochlea of the chicken are replaced. New cells appear to be produced by mitosis of supporting cells that survive at the lesion site and do not divide in the absence of trauma. This trauma-induced division of normally postmitotic cells may lead to recovery from profound hearing loss.

Hair cells are the mechanoreceptors that transduce acoustic stimuli into electrical activity in the ear. Disease, exposure to loud sound, treatment with antibiotics, and processes associated with aging can cause hair cells to die, which results in a loss of hearing (*1*). The hair cells in the cochleae of birds and mammals are produced during the first two-thirds of embryogenesis (*2*), and it has been thought that any subsequent losses lead to permanent deficits. However, in some fish and amphibians hair cells are produced throughout life and may contribute to self-repair (*3*). Recently, we have found that sound-induced damage resulting in the complete loss of the stimulus-transducing stereocilia bundles of hair cells in chickens can be reversed by the growth of new stereocilia bundles (*4*); this observation has been confirmed by other investigators (*5*). Counts of hair cells in histological sections also have shown recovery after an aminoglycoside was administered in chickens (*6*). These findings suggest that regeneration dependent on the production of replacement hair cells may occur in the avian cochlea.

We have investigated the potential regeneration of hair cells by exposing small groups of 9- to 13-day-old chickens to a loud tone, sufficient to cause hair cell loss (*7*). Since damage varies greatly with small changes in sound intensity, one chicken from each group was killed and the cochleae were fixed immediately after the acoustic treatment; only groups with moderate damage were used. Other chickens from each group were allowed to survive for 10 days after the treatment and were administered $[^3H]$thymidine. This radioactive tracer is incorporated into replicating DNA, allowing cells that are mitotically active to be identified later by autoradiography (*7*).

The crescent-shaped sensory epithelium in the chicken cochlea contains a dense population of hair cells, which have surface stereocilia bundles that are stimulated by sound in a high to low pitch gradient from the proximal to the distal end. The other cells in this epithelium are supporting cells, which have microvilli-covered surfaces that are normally interposed as thin lines between the hair cells (Fig. 1A).

When we exposed chickens to a tone of 1.5 kHz at 115- to 120-dB sound pressure level (SPL) for 48 hours, lesions were produced at a consistent location in the proximal half of this epithelium (Fig. 1B). In ears fixed immediately after sound exposure, stereocilia bundles were missing in the lesioned area, and the surface was covered by scattered cells that appeared to have been extruded from the epithelium. Some cells possessed stereocilia bundles that identified them as hair cells. The positions that hair cell surfaces normally would have occupied were filled by the expanded surfaces of supporting cells. During the 10 days after the treatment, the lesioned area gradually returned to normal as stereocilia bundles reappeared, differentiated, and grew larger, in a manner resembling their embryogenesis (*8*), so that the site of the lesion became almost indistinguishable from the same site in control epithelium (*4*) (Fig. 1, C to F).

Autoradiographic localization of DNA that incorporated the radioactive thymidine demonstrated that the damage produced by the acoustic treatment had stimulated mitotic replication of cells. At the lesion site, the

J. T. Corwin, Department of Zoology and Békésy Laboratory of Neurobiology, Pacific Biomedical Research Center, University of Hawaii, Honolulu, HI 96822.
D. A. Cotanche, Department of Anatomy, Boston University School of Medicine, Boston, MA 02118.